Hindawi Publishing Corporation
Advances in Materials Science and Engineering
Volume 2015, Article ID 376173, 8 pages
http://dx.doi.org/10.1155/2015/376173

Research Article

Fabrication of UO_2 Porous Pellets on a Scale of 30 kg-U/Batch at the PRIDE Facility

Sang-Chae Jeon, Jae-Won Lee, Ju-Ho Lee, Sang-Jun Kang, Kwang-Yun Lee, Yung-Zun Cho, Do-Hee Ahn, and Kee-Chan Song

Korea Atomic Energy Research Institute, Daedeok-daero 989-111, Yuseong-gu, Daejeon 305-353, Republic of Korea

Correspondence should be addressed to Sang-Chae Jeon; scjeon@kaeri.re.kr

Received 1 July 2015; Accepted 11 August 2015

Academic Editor: Kisor K. Sahu

In the pyroprocess integrated inactive demonstration (PRIDE) facility at the Korea Atomic Energy Research Institute (KAERI), UO_2 porous pellets were fabricated as a feed material for electrolytic reduction on an engineering scale of 30 kg-U/batch. To increase the batch size, we designed and modified the corresponding equipment for unit processes based on ceramic processing. In the course of pellet fabrication, the correlation between the green density and sintered density was investigated within a compaction pressure range of 106–206 MPa, in terms of the optimization of processing parameters. Analysis of the microstructures of the produced UO_2 porous pellets suggested that the pellets were suitable for feed material in the subsequent electrolytic reduction process in pyroprocessing. This research puts forth modifications to the process and equipment to allow the safe mass production of UO_2 porous pellets; we believe these results will have immense practical interest.

1. Introduction

Nuclear reprocessing is the process of chemically treating spent nuclear fuel to recover plutonium (Pu) and uranium (U). The aqueous process, PUREX, has conventionally been used for this purpose. However, pyroprocessing has recently emerged as one of the key technologies that can reduce nuclear waste while improving the efficiency of resource use in the nuclear fuel cycle. This is because, among other advantages over PUREX, pyroprocessing is less proliferative as it does not enable the separation of Pu from other impurities [1]. Pyroprocessing is a process that starts with the head-end process, followed by electrolytic reduction, electrorefining, electrowinning, and salt purification [1–3].

The head-end process includes chopping, mechanical or oxidative decladding, and high-temperature voloxidation as unit processes. During the head-end process, uranium and transuranic (TRU) elements are recovered from spent fuel, while fission products such as Kr, Xe, H-3, C-14, Cs, and I are removed [4–6]. Another important goal of the head-end process is the fabrication of a proper feed material for the subsequent electrolytic reduction process. The feed material can take on different physical forms depending on the decladding method used: mechanical decladding results in crushed particles, whereas oxidative decladding results in porous pellets or granules. Compared to mechanical decladding, oxidative decladding results in a high recovery rate of the fuel material from rod-cuts [3]. However, during the oxidative decladding process, uranium oxide undergoes a change in phase from a UO_2 pellet to a U_3O_8 powder. In this viewpoint, the UO_2 porous pellet form, which can be prepared from the U_3O_8 powder via ceramic processing, has attracted much interest as a promising feed form for the following electrolytic reduction [6–9].

The fabrication of a UO_2 porous pellet involves pelletizing and sintering of U_3O_8 pellets at high temperature under a H_2-containing atmosphere [6]. In this regard, there have been many studies that have investigated the reduction behaviors and microstructural variations of U_3O_8 under reducing atmosphere [10–15]. However, the majority of such investigations have been carried out on a lab scale. Therefore, in order to achieve engineering-scale production (50 kg-U/batch), for example, at the PRIDE facility [9], it is necessary to determine if the fabrication process and the corresponding equipment need to be modified to suit mass production.

Table 1: Fabrication process of UO_2 porous pellets and its chemical/physical form during the various stages.

Process	Starting material		Oxidation		Mixing		Pelletizing		Sintering
Chemical/ physical Form	UO_2/ dense pellet	→	U_3O_8/ powder	→	U_3O_8 + EBS[a]/ powder	→	U_3O_8 + EBS[a]/ pellet	→	UO_2/ porous pellet

[a]Ethylene bis stearamide, $(CH_2NHC(O)C_{19}H_{35})_2$.

In the present experiment, based on the literature and conventional ceramic processing, a fabrication process was adapted to meet the needs of the fabrication scale in PRIDE facility: oxidation, mixing, pelletizing, and sintering. Towards this end, the fabrication equipment was newly designed and improved by introducing new structures. In addition, the relationship between the green density and sintered density under compaction pressure was investigated in the course of mass production. From a practical aspect, the results of this investigation can be employed to the mass production of UO_2 porous pellets, which can be used as a feed material for the subsequent electrolytic reduction process.

2. Materials and Methods

2.1. Fabrication of Porous Pellets. Similar to conventional ceramic processing, the fabrication of UO_2 porous pellets in the PRIDE facility involves four sequential processes: oxidation, mixing, pelletizing, and sintering. The fabrication process of the porous pellets and the chemical/physical form of the produced uranium oxides after each process are summarized in Table 1. Considering the purpose of the PRIDE facility, the fabrication equipment was designed to accommodate a capacity of 50 kg-U/batch; a schematic drawing of this equipment is shown in Figure 1. The porous UO_2 pellets were fabricated in the PRIDE facility as follows: UO_2 pellets with a diameter of 8.05 mm, a height of 10.08 mm, and a weight of 5.20 g were prepared as the starting material. The geometrical density of UO_2 pellets was about 92.47% on average, much higher than the theoretical density of UO_2, 10.96 g/cm^3. The UO_2 pellets were oxidized to U_3O_8 powder at 480°C for 16 h under a 75% O_2-Ar atmosphere in a rotating drum furnace, which was equipped with a double chamber: an inner chamber made of INCONEL 600 and an outer chamber of SUS 304 stainless steel. A schematic drawing and a photograph of the rotating drum furnace are shown in Figure 1(a). On the inside wall of the inner chamber, a spiral screw structure is formed to allow transport of the UO_2 feed pellets and/or produced U_3O_8 powders back and forth by rotating the chambers. After complete oxidation of the UO_2 pellets, the oxidized U_3O_8 powder was recovered by reverse rotation of the chambers. The recovered U_3O_8 powder was mixed with 2 wt% of acrawax (ethylene bis stearamide (EBS), $C_{38}H_{76}O_2N_2$, CAS #: 110-30-5) by using a tubular mixer for 30 min. Acrawax is a well-known lubricant used to minimize die wall friction during the subsequent pelletizing process. The powder mixture containing EBS was then pressed into a pellet shape using the rotary press machine shown in Figure 1(b). A schematic drawing of the driving part of the rotary press shows 13 sets of die and punches (Figure 1(b)). In a single rotation cycle, U_3O_8 powder is injected into the hole of the die, followed by compaction of the filled powder in the die by the upper and lower punches and ejection of the pelletized U_3O_8; this cycle can be repeated continuously. The hole of the die used in this experiment was designed to be 6.6 mm wide, and the rotation speed of the rotary press was optimized to be 5 rpm during the pelletizing process. The green pellets obtained after pressing were sintered and reduced in a vertical-type sintering furnace that helped to minimize the temperature gradient throughout the heating zone. The heating elements penetrating the ceiling surface of the furnace chamber allow the samples to be completely surrounded by the heating element. The green pellets were put into five zirconia crucibles, which can contain ~13 kg of U_3O_8 pellets, and then sintered at 1350°C for 12 h under 4% H_2-Ar atmosphere.

2.2. Characterization of Porous Pellets. The microstructures of the U_3O_8 powders and UO_2 pellets were observed by scanning electron microscopy (SEM, Philips XL-30, Netherlands) after polishing using diamond paste. The pore sizes and size distributions were measured from the SEM images using the image processing software, Matrox Inspector 2.1 (Matrox Inc. Canada). The crystal structure of the fabricated UO_2 pellets was examined using X-Ray Diffraction (XRD, Rigaku Mini-Flex, Japan). The XRD experiments were performed over the 2θ range of 20–80° and at a scan speed of 6°/min and a step size of 0.01°. The pellets were crushed into powder form in an agate mortar and pestle prior to the measurements.

3. Results and Discussion

Figure 2 shows the variations in the temperature and O_2 concentration during the oxidation process of UO_2 to U_3O_8 in a rotating drum furnace (Figure 2(a)) and macro/microscopic images of the resultant oxidized U_3O_8 powder (Figure 2(b)). The oxidation temperature was determined based on a previous report on the oxidation of UO_2 to U_3O_8 [16]. This was done taking into account the temperature difference measured during the preliminary test between the two different positions of the rotating drum furnace: temperature of heating element (T_{he}) and inside chamber (T_{inside}). Through the heat treatment at 470–480°C for 16 h, fine U_3O_8 powders were produced without significant agglomerates, as shown in Figure 2(b), indicating homogeneous oxidation of UO_2 into U_3O_8.

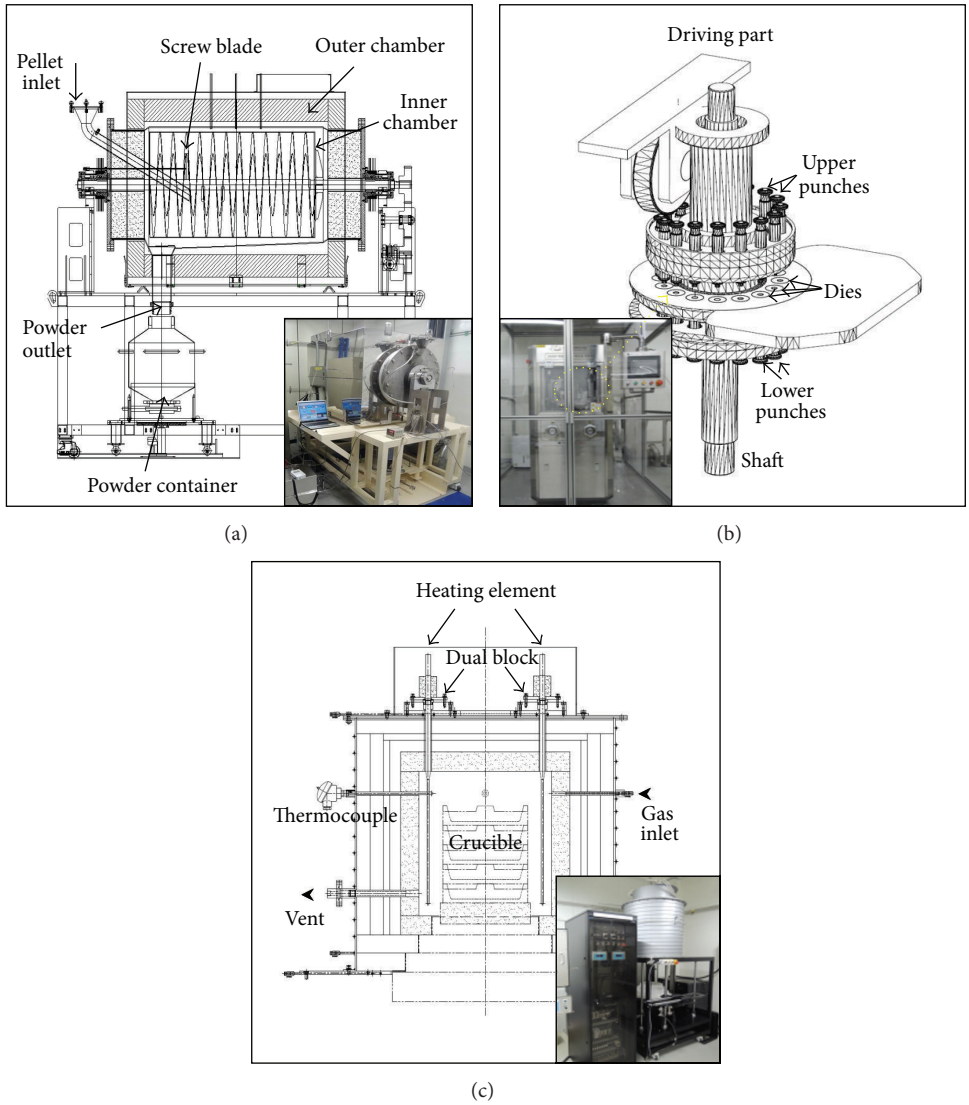

Figure 1: Schematic drawings and photographs of (a) rotating drum furnace, (b) driving part of rotary press, and (c) sintering furnace constructed in PRIDE.

During the oxidation, the phase change is accompanied by volumetric expansion (~23.6%) due to the difference in density between the two phases: 10.96 g/cm^3 for UO_2 and 8.37 g/cm^3 for U_3O_8 [13]. The U_3O_8 powder particles, therefore, become popcorn shaped. In our experiment as well, the U_3O_8 powder particles were popcorn shaped, with an average particle size of 4.63 μm, as shown in Figure 2(b) [17, 18]. Both fine particle size and uniform phase of the produced U_3O_8 powder are conditions necessary for securing good compactibility during the following pelletizing process. Before the pelletizing process, 0.2 wt% of acrawax was added to the U_3O_8 powders. Acrawax is a well-known lubricant material in powder metallurgy, and it reduces the friction between the die and the wall while improving the mechanical strength of the green pellet [19]. After addition of the acrawax, the powders were mixed using a tubular mixer for 30 min to improve the uniformity of the powders.

The mixed U_3O_8 powders were then compacted into pellets using a rotary press, as shown in Figure 2(b). The rotary press exhibited excellent production yield: 3,500 pellets per hour (7 kg-U/h). The rough shape of the U_3O_8 powder indicates that it has poor flowability, which leads to the failure of uniform die filling during the pelletizing process. To improve the flowability, in this experiment, a mechanical feeder was installed. Figure 3(a) shows a schematic of the mechanical feeder attached at the feeding part of the rotary press. It consists of three impellers and a powder scraper, which allow a constant amount of U_3O_8 powders to be filled in the rotating dies. With the rotary press machine, around 30 kg of U_3O_8 powders were compressed into green pellets, as shown in Figure 3(b).

With an aim of optimizing the processing parameters in the pelletizing experiment, the effect of compaction pressure on the density of green pellets was examined. The compaction

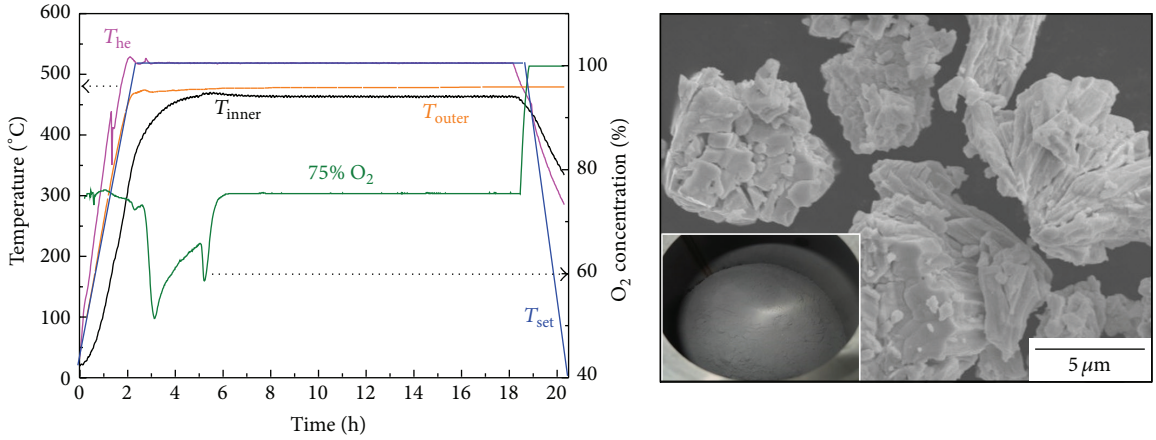

(a) (b)

FIGURE 2: Experimental conditions and results of oxidation process: (a) variations in temperature and O_2 concentration and (b) produced U_3O_8 powder.

(a) (b)

FIGURE 3: Modification of the equipment and results of pelletizing process: (a) schematic drawings and a photograph of the mechanical feeder attached to rotary press and (b) produced U_3O_8 green pellets.

pressure could be controlled by regulating the amount of U_3O_8 powder filled into die hole and the pressing depth of upper punch. In this case, the compaction pressure ranged from approximately 100 to 200 MPa. The density of pellets increased linearly with the compaction pressure in the range of 60.33 to 68.14% TD, as listed in Table 2. The geometrical information and green density values for pelletization under different pressures are also summarized in Table 2. The pellets have similar size and weight, with little standard deviation in the values, thus indicating that a uniform amount of powders was filled and uniform force was applied during the pelletizing process using a rotary press machine. Figure 4 shows photographs of the green pellets pressed under different compaction pressure values. It is evident that the surface of the pellets becomes smoother with increasing compaction pressure.

To ensure that the U_3O_8 green pellets are suitable as feed for electrolytic reduction, they must be sintered and reduced to UO_2 phase by heat treatment in the furnace. As shown in Figure 1(c), a vertical-type furnace was constructed for heat treatment of the green pellets (50 kg/batch). A vertical-type furnace was used in order to minimize the temperature gradient throughout the heating zone. The sample loaded at the center of the furnace was surrounded by the heating element. To secure mechanical stability up to high temperatures, the green pellets were placed in zirconia crucible that was 320 mm in diameter and 10 mm thick. Each crucible contained ~13 kg of U_3O_8 pellets and could be stacked tightly on another crucible.

Figure 5 shows the programmed and measured temperature variations during sintering of the U_3O_8 green pellets. The sintering was conducted at 1350°C for 12 h under a reducing atmosphere using a gas containing hydrogen (4% H_2-Ar balanced). The thermal history includes dewaxing treatment at 700°C for 1 h to remove the added acrawax. The retarded heating and cooling rate could be attributed to

Table 2: Green and sintered density and % TD (theoretical density) of pellets under different compaction pressures.

Compaction pressure (MPa)	Pellet height (mm)	Pellet weight (g)	Green density (g/cm^3)	% TD[a] (%)
106 {33}	6.78 {0.03}	1.17 {0.03}	5.05 {0.13}	60.33 {1.51}
160 {43}	6.34 {0.03}	1.19 {0.03}	5.50 {0.14}	65.73 {1.63}
206 {52}	6.02 {0.06}	1.17 {0.03}	5.70 {0.11}	68.14 {1.37}

[a]Theoretical density compared to U_3O_8 (8.37 g/cm^3).
{} Standard deviation.

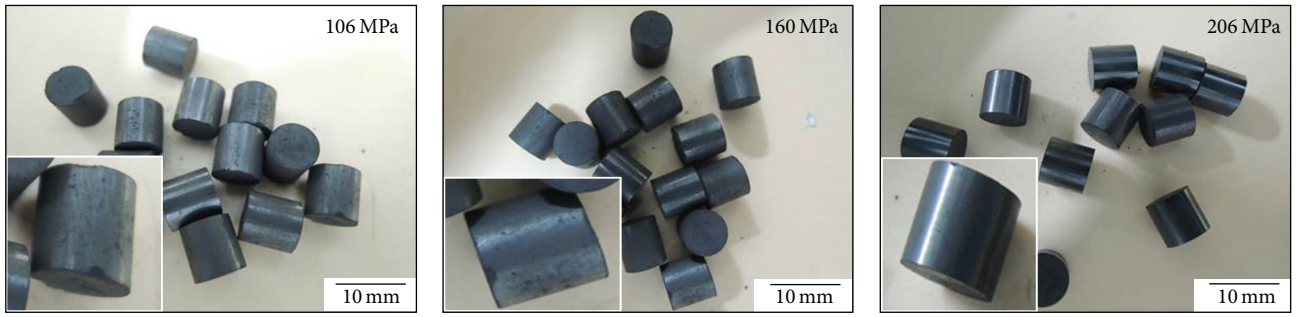

(a) (b) (c)

Figure 4: Green pellets pressed under different pressures: (a) 106, (b) 160, and (c) 206 MPa.

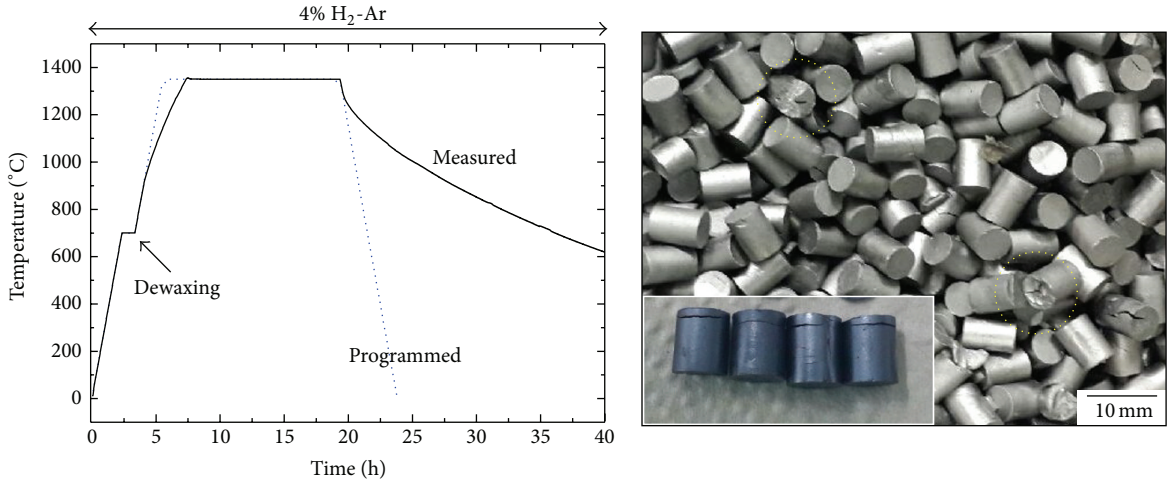

(a) (b)

Figure 5: Experimental conditions and results of oxidation process: (a) thermal profile of sintering process and (b) produced UO_2 sintered pellets. The inset in (b) and dashed circles indicate delamination defects.

the thick refractory ceramics coated inside the heating zone. Figure 5(b) shows the sintered UO_2 pellets with a scale of 30 kg-U/batch. Among the produced pellets, delamination cracks are observed at the end of some pellets, as shown in the inset photograph. The dashed circles in Figure 5(b) show the pellets that were crushed owing to the delamination cracks. The delamination crack is known to result from severe friction between the die and the wall during the pelletizing process [20]. When cracks are formed in the pellets, dust particles (<45 μm), which escape the cathode basket and infiltrate into the molten salt in the electrolytic reduction process, can be formed. The crack formation can be avoided by further optimizing the processing conditions, such as the amount of acrawax, mixing time, and compaction pressure.

Figure 6 shows the XRD patterns of the sintered pellets extracted from different crucibles: top and bottom floor. All patterns are similar to that of the UO_2 phase, without any second phase. This indicates that all of the sintered pellets have the UO_2 phase, irrespective of their position in the furnace during the sintering. It also implies that the reduction

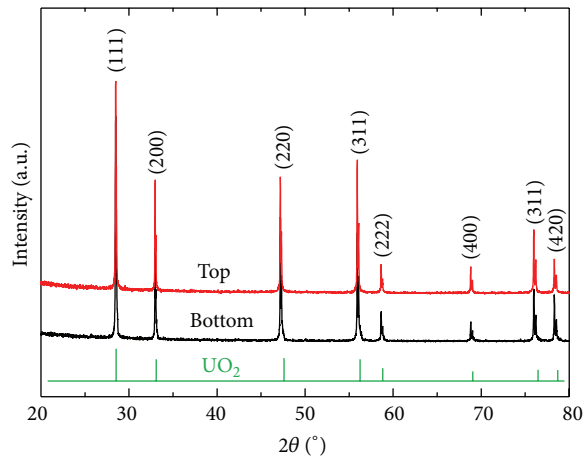

Figure 6: XRD patterns of sintered pellets extracted from the bottom and top crucibles.

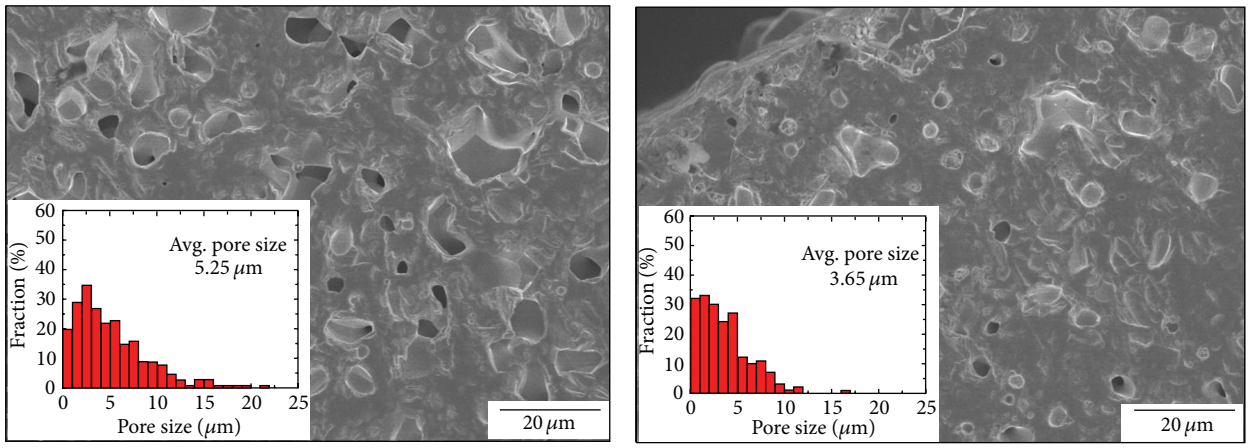

Figure 7: SEM micrographs and measured pore size distributions of sintered pellet: (a) inside and (b) surface.

of U_3O_8 to UO_2 was completed during the previous sintering process.

Figure 7 shows SEM micrographs of different positions in a pellet: inside and surface. The pore structures at the center/surface of the porous pellet were clearly observed after mechanical polishing but with no etching. Except a slight difference in the size of the pores and their connectivity, both from the inside and from the surface, a porous microstructure with interconnected micropores is clearly seen in the SEM micrographs. Compared to the pores on the surface, the pores inside the pellets were larger and more interconnected. The average pore size inside and on the surface of the pellets was 5.25 and 3.65 μm, respectively. This could be attributed to the preceding densification of the surface region, resulting in the escape of gas trapped in the pores deep inside the pellet.

Figure 8 shows the relationship between the green density of the U_3O_8 pellets and the sintered density of the UO_2 pellets with respect to the compaction pressure. In the following electrolytic reduction process, the density of a porous pellet is one of the major factors determining the reduction efficiency [20]. Generally, the sintered density of UO_2 pellets strongly depends on the green density of U_3O_8 pellets, which is determined by the compaction pressure in the pelletizing process. Therefore, to fabricate porous UO_2 sintered pellets within a suitable density range, the relationship between the compaction pressure, green density of U_3O_8 pellets, and sintered density of UO_2 pellets should be clarified. In this experiment, the following linear relationship was obtained in the compaction pressure range from 106 to 206 MPa:

$$\mathrm{SD}\,(\%) = 0.35\mathrm{GD}\,(\%) + 39.87\,(\%)\,, \tag{1}$$

where SD and GD are the percentages of sintered density and green density, respectively. This provides technical data for the fabrication of UO_2 porous pellets in large batches and can help in ensuring the quality assurance and quality control (QA/QC) of the porous pellets.

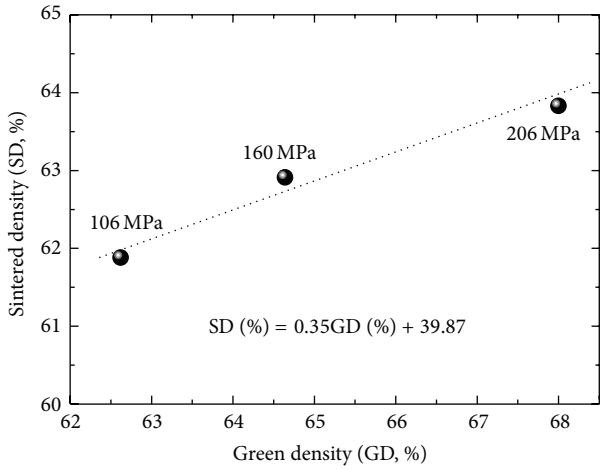

Figure 8: Relationship between green density (GD) and sintered density (SD) with compaction pressure.

4. Conclusions

UO_2 porous pellets, which are promising as a feed material for the electrolytic reduction process in pyroprocessing, were fabricated in the PRIDE facility at an engineering scale. The fabrication processing was based on conventional ceramic processing, which consists of oxidizing, pelletizing, and sintering. To meet the demand for scaling up, three kinds of fabrication equipment were constructed, and the drawbacks in scaling up were addressed at the stage of design and fabrication. A screw structure in the rotating drum furnace helps to convey a large amount of powders/pellets by rotating the chambers in the oxidation process, a mechanical feeder improves the flowability of the U_3O_8 powders into the hole of dies during the pelletizing process, and a vertically penetrating heating element structure reduces the temperature gradient throughout the large space during the sintering process. In addition, this paper clarifies the relationship between green density, sintered density, and the compaction pressure in terms of the optimization of processing parameters as a practical aspect of the fabrication of UO_2 porous pellets.

Conflict of Interests

The authors declare that they have no conflict of interests regarding the publication of this paper.

Acknowledgment

This work was supported by the National Research Foundation of Korea (NRF) grant funded by the Korea government (MEST) (no. 2012M2A8A5025696).

References

[1] K.-C. Song, H. Lee, J.-M. Hur, J.-G. Kim, D.-H. Ahn, and Y.-Z. Cho, "Status of pyroprocessing technology development in Korea," *Nuclear Engineering and Technology*, vol. 42, no. 2, pp. 131–144, 2010.

[2] J.-H. Yoo, C.-S. Seo, E.-H. Kim, and H.-S. Lee, "A conceptual study of pyroprocessing for recovering actinides from spent oxide fuels," *Nuclear Engineering and Technology*, vol. 40, no. 7, pp. 581–592, 2008.

[3] H. Lee, G.-I. Park, K.-H. Kang et al., "Pyroprocessing technology development at KAERI," *Nuclear Engineering and Technology*, vol. 43, no. 4, pp. 317–328, 2011.

[4] J. G. Asquith and L. F. Grantham, "A low-decontamination approach to a proliferation-resistant fuel cycle," *Nuclearear Technology*, vol. 41, no. 2, pp. 137–148, 1978.

[5] J. Y. Colle, J.-P. Hiernaut, D. Papaioannou, C. Ronchi, and A. Sasahara, "Fission product release in high-burn-up UO_2 oxidized to U_3O_8," *Journal of Nuclear Materials*, vol. 348, no. 3, pp. 229–242, 2006.

[6] Y. Sakamura and T. Omori, "Electrolytic reduction and electrorefining of uranium to develop pyrochemical reprocessing of oxide fuels," *Nuclear Technology*, vol. 171, no. 3, pp. 266–275, 2010.

[7] E.-Y. Choi, J.-M. Hur, I.-K. Choi et al., "Electrochemical reduction of porous 17 kg uranium oxide pellets by selection of an optimal cathode/anode surface area ratio," *Journal of Nuclear Materials*, vol. 418, no. 1–3, pp. 87–92, 2011.

[8] H.-S. Lee, G.-I. Park, J.-W. Lee et al., "Current status of pyroprocessing development at KAERI," *Science and Technology of Nuclear Installations*, vol. 2013, Article ID 343492, 11 pages, 2013.

[9] S.-C. Jeon, J.-W. Lee, S.-J. Kang et al., "Temperature dependences of the reduction kinetics and densification behavior of U_3O_8 pellets in Ar atmosphere," *Ceramics International*, vol. 41, no. 1, pp. 657–662, 2014.

[10] H. Chevrel, P. Dehaudt, B. Francois, and J. F. Baumard, "Influence of surface phenomena during sintering of overstoichiometric uranium dioxide UO_{2+x}," *Journal of Nuclear Materials*, vol. 189, no. 2, pp. 175–182, 1992.

[11] M. Pijolat, C. Brun, F. Valdivieso, and M. Soustelle, "Reduction of uranium oxide U_3O_8 to UO_2 by hydrogen," *Solid State Ionics*, vol. 101-103, no. 1, pp. 931–935, 1997.

[12] C. Brun, F. Valdivieso, M. Pijolat, and M. Soustelle, "Reduction by hydrogen of U_3O_8 into UO_2: nucleation and growth, influence of hydration," *Physical Chemistry Chemical Physics*, vol. 1, no. 3, pp. 471–477, 1999.

[13] K. W. Song, K. S. Kim, and Y. H. Jung, "Densification behavior of U_3O_8 powder compacts by dilatometry," *Journal of Nuclear Materials*, vol. 279, no. 2-3, pp. 356–359, 2000.

[14] F. Valdivieso, M. Pijolat, M. Soustelle, and J. Jourde, "Reduction of uranium oxide U_3O_8 into uranium dioxide UO_2 by ammonia," *Solid State Ionics*, vol. 141-142, pp. 117–122, 2001.

[15] J. H. Yang, Y. W. Rhee, K. W. Kang, K. S. Kim, K. W. Song, and S. J. Lee, "Formation of columnar and equiaxed grains by the reduction of U_3O_8 pellets to UO_{2+x}," *Journal of Nuclear Materials*, vol. 360, no. 2, pp. 208–213, 2007.

[16] F. Valdivieso, V. Francon, F. Byasson, M. Pijolat, A. Feugier, and V. Peres, "Oxidation behaviour of unirradiated sintered UO_2 pellets and powder at different oxygen partial pressures, above 350°C," *Journal of Nuclear Materials*, vol. 354, no. 1-3, pp. 85–93, 2006.

[17] K. W. Song and M. S. Yang, "Formation of columnar U_3O_8 grains on the oxidation of UO_2 pellets in air at 900°C," *Journal of Nuclear Materials*, vol. 209, no. 3, pp. 270–273, 1994.

[18] J. H. Yang, K. W. Kang, K. S. Kim, Y. W. Rhee, and K. W. Song, "Recycling process for sinter-active U_3O_8 powders," *Journal of Nuclear Science and Technology*, vol. 47, no. 6, pp. 538–541, 2010.

[19] M. M. Baum, R. M. Becker, A. M. Lappas et al., "Lubricant pyrolysis during sintering of powder metallurgy compacts," *Metallurgical and Materials Transactions B*, vol. 35, no. 2, pp. 381–392, 2004.

[20] J. S. Reed, *Principles of Ceramics Processing*, John Wiley & Sons, New York, NY, USA, 1996.